

Highly selective copper ion imprinted clay/polymer nanocomposites designed by visible light radical photopolymerization

Radhia Msaadi^a, Gorkem Yilmaz^b, Andrit Allushi^b, Sena Hamadi^c,
Salah Ammar^a, Mohamed M. Chehimi^{c,*}, Yusuf Yagci^{b,*}

^aUniversité de Gabès, Faculté des Sciences, Unité de Recherche Électrochimie, Matériaux et Environnement UREME (UR17ES45), Gabès, Tunisia
radhiaradhia44@gmail.com (RM), salah.ammar@fsg.rnu.tn (SA)

^bIstanbul Technical University, Department of Chemistry, Maslak, Istanbul 34469, Turkey
a.gorkemyilmaz@gmail.com (GY), andrit.allushi@chem.lu.se (AA), yusuf@itu.edu.tr (YY)

^cUniversité Paris Est, ICMPE (UMR 7182), CNRS, UPEC, F-94320 Thiais, France
hamadi@icmpe.cnrs.fr (SH), chehimi@icmpe.cnrs.fr (MMC)

Abstract

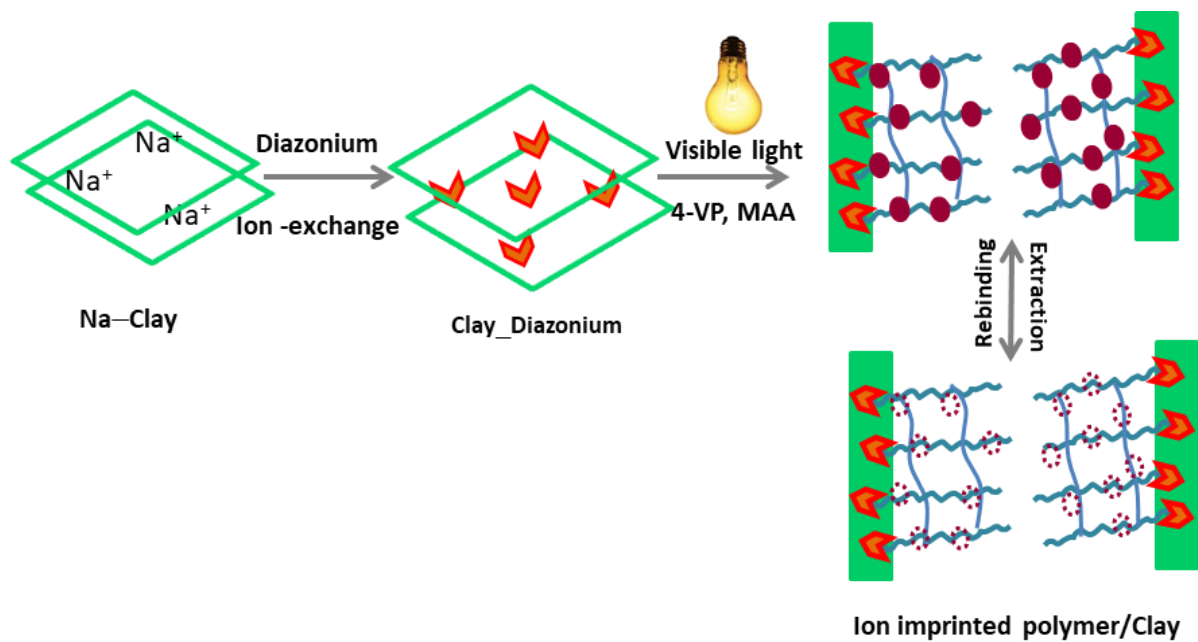
There is an urgent demand worldwide for the development of highly selective adsorbents and sensors of heavy metal ions and other organic pollutants. Within these environmental and public health frameworks, we are combining the salient features of clays and chelating polymers to design selective metal ion adsorbents. Towards this end, the ion imprinting approach has been used to develop a novel nanohybrid material for the selective separation of Cu²⁺ ions in aqueous solution. The Cu²⁺-imprinted polymer/ montmorillonite nanocomposite (IIP/Mt) and non-imprinted polymer/montmorillonite nanocomposite (NIP/Mt) were prepared by radical photopolymerization process in the visible light. Ion imprinting was indeed important as the recognition of copper ions by IIP/Mt was significantly superior to that of NIP/Mt that is the nanocomposite synthesized in the same way but in the absence of Cu²⁺ ions. The adsorption process as batch study was investigated under the experimental condition affecting same parameters such as contact time, concentration of ions metals and pH. The adsorption capacity of Cu²⁺ ions is maximized at pH 5. Removal of Cu²⁺ ion achieved equilibrium within 15 minutes; the results obtained were found to be fitted by the pseudo-second order kinetics model. The equilibrium process was well described by the Langmuir isothermal model and the maximum adsorption capacity was found to be 23.6 mg/g.

Keywords: clay; diazonium salt; ion imprinted polymers; radical photopolymerization; visible light; adsorption; copper ions.

Corresponding authors:

Mohamed M. Chehimi: chehimi@icmpe.cnrs.fr; Yusuf Yagci: yusuf@itu.edu.tr

Graphical abstract



1. Introduction

There is a global concern of heavy metal pollution of the environment with a high risk for these elements to enter the food chain via natural and anthropogenic routes [1]. Heavy metal ions pollutants affect humans after ingestion of water and food [2,3]. For example, children are particularly vulnerable to the neurotoxic effects of lead, and exposure, even at relatively low levels, may cause serious, and in some cases irreversible, neurological damage [4].

For these reasons, heavy metal pollution is regarded as one of the most challenging global problems and requires combined actions such as detections at minute levels and removal at a separation/filtration stage using high capacity selective adsorbents. The first issue of the problem can be addressed by develop highly sensitive and selective sensors for a YES/NO response of the sensors to indicate whether or not a sample is contaminated by heavy metals; ideally the output response is processed to return a quantitative value of the metal ion concentration in the target sample [5,6]. In addition to sensitive devices, the second important issue is to develop high capacity adsorbents to remove or to pre-concentrate heavy metals in order to have a complete picture of the pollution by metal ions from the surface physico-chemical point of view. Towards this end, clays can be regarded as natural inorganic “sponges” to retain heavy metal ions [7,8]. However, aluminosilicates are negatively charged and retention of heavy metal ions could be achieved through cation exchange reactions. In this sense, clays are not selective [8] and organo-modification permits to impart to clays functional groups for the specific retention of metal ions. For example, NH_2 , SH , $\text{C}=\text{C}$, calixarene, crown-ethers and cryptand, dendrimer among others have been attached to clays via ammonium salts, diazonium salts, silane coupling agents or other strategies [9,10,11,12,13,14,15,16,17]. In a more elaborated picture, clay/polymer nanocomposites can also be envisaged if the polymer possesses pendant functional groups able to complex metal ions [18], yet selectivity remains challenging. Some of us reported various synthetic approaches for the syntheses of clay-polymer nanocomposites including free radical, cationic and ring-opening polymerizations and click chemistry [19,20,21,22,23]. By incorporating suitably selected functional groups onto clay surface a wide variety of polymerization systems can successfully be applied in an *in situ* manner.

To push the frontiers of selectivity further, a smart strategy consists of making clay/ion imprinted polymer nanocomposites [24,25], therefore combining the best of the two worlds: high capacity mineral adsorbent [26] and highly selective organic material *c.a.* ion imprinted polymers [27,28,29,30,31]. We have previously demonstrated that such materials can be designed by UV-triggered radical photopolymerization of functional and crosslinker in the

presence of organo-clay [32]. In a unique approach, we have efficiently organo-modified clay using the versatile aryl diazonium instead of ammonium salts or silane coupling agents bearing photoinitiator.

Yet, the original design of nanohybrids we have reported recently requires UV light initiation. Instead, herein we simplify the process by triggering radical photopolymerization under visible light using diazonium-modified clay as a macro-initiator and camphorquinone (CQ) as photosensitizer. CQ is indeed a very efficient photosensitizer for generating ultrathin polymer coatings by simulated sunlight-induced surface-confined radical photopolymerization [33]. To the very best of our knowledge, this strategy has never been reported previously, it is highly interesting simply because the clay/IIP nanocomposite can be designed using natural day or simulated day light or white light.

Herein, montmorillonite was first cation exchanged with a diazonium compound bearing dimethyl amino groups to provide a macro-photoinitiator, and visible light radical photopolymerization was conducted in the presence of the modified clay, the monomers (4-vinylpyridine, (VP) methacrylic acid (MA), CQ and the heavy metal ions. Thorough rinsing of the final product, permitted to remove the metal ions and to create the artificial receptor sites for the selective recognition of copper.

2. Experimental

2.1. Chemicals and Reagents

All chemical reagents and materials were purchased from Aldrich and used without further purification. Milli-Q Plus water purification system was employed to prepare deionized water.

2.2. Instrumentation and characterization

X'Pert PRO (PANalytical) instrument fitted with a Co K α X-ray source (1.789 Å) was employed to record the diffraction patterns of the samples.

Infrared spectra were recorded using a Nicolet Magna-IR 550 spectrometer in the attenuated total reflection (ATR) mode, in the 4000-450 cm⁻¹ range.

AK Alpha instrument (Thermo) fitted with a monochromated Al K α X-ray source (h ν = 1486.6 eV, spot size = 400 μ m) was used for XPS measurements. Aflood gun was employed for static charge compensation. The analyzer was operated at 80 and 200 eV pass energy for the narrow

regions and survey spectra, respectively. Elemental atomic concentrations were computed using the integrated peak areas and the corresponding sensitivity factors provided by the manufacturer.

The determination of metal ion concentration was performed with Avanta/GBC flame atomic absorption spectrophotometer equipped with a hollow cathode lamp and deuterium background corrector at respective wavelength resonance line using an air-acetylene flame.

2.3. Synthesis of the diazonium salt $\text{Cl}^- \text{N}_2 \text{C}_6\text{H}_4\text{N}=\text{NC}_6\text{H}_4\text{N}-(\text{CH}_3)_2$

N,N-Dimethyl-4,4' azoanilinediazonium salt was prepared as follows: the aromatic amine (4.16 mmol, 1g) is suspended in a hydrochloric acid and distilled water 50/50 v/v%. The mixture was cooled in an ice bath, and then 1 equivalent of sodium nitrite was slowly added. The mixture was stirred for 15 min. IR characterization of the diazonium salt N_2^+ , 2204cm^{-1} .

2.4. Diazonium modification of montmorillonite

To an aqueous suspension of clay (100 mg dispersed in 10 ml of de-ionized water) we added dropwise an aqueous solution of diazonium salt (500 mg in 10 ml of deionized water). The intercalated clay was washed thoroughly with deionized water and dried at 60°C overnight.

2.5. Synthesis of Cu^{2+} -IIP/Mt nanocomposite

The IIP/Mt nanocomposite was prepared in two major sequential steps. First, 1 equivalent of template $\text{Cu}(\text{NO}_3)_2$, 2 equivalents of 4-vinylpyridine (4-VP, 0.431mL) and 2 equivalents of methacrylic acid (MA, 0.339mL) were dissolved in (4ml/4ml v/v) DMF and water in a glass tube, and were kept under stirring for 1 hour. Then, 1 equivalent of cross-linker (EDGMA, $V=0.377\text{ml}$), 41 mg of CQ (8 wt.% of the monomer 4-VP or MAA) and 200 mg of modified clay (Mt-DZ) by diazonium (dimethyl-4,4-azoaniline diazonium) were added in glass tube. The glass tube was purged with nitrogen for 15 min. The mixture was irradiated using a Ker-vis blue photoreactor equipped with six lamps (Philips TL-D 18 W) emitting light nominally at 400-500 nm at room temperature for 4 hours.

Template ion (Cu^{2+}) was removed by washing the nanocomposite in HNO_3 (0.1M) in order to obtain specific artificial recognition sites within the IIP/Mt nanocomposites.

The same clay-polymer nanocomposite was prepared but in the absence of copper; it is noted NIP/Mt for non-imprinted polymer/montmorillonite.

2.6. Metal ion adsorption

Adsorption of Cu^{2+} on the IIP/Mt nanocomposite and NIP/Mt nanocomposite was examined using batch experiments. To prepare adsorption isotherms, a series of samples containing 4mg of an appropriate IIP/Mt and NIP/Mt as equilibrated with 10mL solution containing various concentrations (5- 20 mg/l) of Cu^{2+} . The solution was shaken at room temperature for 2h. After adsorption, the mixture was isolated by centrifugation, then filtered through a 0.45 μm membrane filter and examined with atomic absorption spectroscopy (AAS). The adsorption amount (q_e ; mg/g) was calculated using:

$$q_e = \frac{(C_0 - C_e)V}{m} \quad (1)$$

Where C_0 and C_e are initial and equilibrium concentration (mg/L), m is the sorbent mass (g), and V is the solution volume (L).

Kinetic studies were conducted to determine the adsorption rate of Cu^{2+} from water samples as follows: 4mg of each sorbent were dispersed in 10mL solution containing the same initial Cu^{2+} concentration of 20 mg/L. Each mixture was continuously batch oscillated at room temperature for 5,10,15,30,60,90 and 120 min. After each time period, solutions were filtered and analyzed by AAS to determine the concentration of Cu^{2+} in the supernatant.

To investigate the effect of pH, 4 mg IIP/Mt and NIP/Mt were added to 20mL sample solutions containing 20 mg/L of Cu(II) ion at pH range 2.0-9.0, respectively, pH values were adjusted by 1mol/L HNO_3 and 1 mol/L NaOH.

2.7. Selectivity experiments

To estimate the selectivity of the ion-imprinted polymer/Mt nanocomposite and their corresponding non-imprinted polymer/Mt nanocomposites materials for copper adsorption, 5mg of the sorbent was added into 10ml of 20mg/L binary solution of $\text{Cu}^{2+}/\text{Zn}^{2+}$, $\text{Cu}^{2+}/\text{Pb}^{2+}$, and $\text{Cu}^{2+}/\text{Fe}^{3+}$ for 1h. The mixture was magnetically stirred at 300 rpm, then left to decant for 15 min, centrifuged, and filtered. Finally, the concentration of copper and the interfering ions was measured by AAS.

The distribution coefficients, K_d (ml/g), of Cu^{2+} , Zn^{2+} , Pb^{2+} , and Fe^{3+} were calculated using equation:

$$K_d = \frac{(C_0 - C_e)V}{C_e m} \quad (2)$$

The selectivity coefficients for the binding of a copper ion in the presence of other competing ions in binary systems were calculated according to the following equations:

$$K = \frac{K_d(\text{Cu}^{2+})}{K_d(\text{M}^{n+})} \quad (3)$$

Where M^{n+} ($n=2$ or 3) represents Cu^{2+} competing ions mentioned above. The coefficients give an indication as to how selective the nanocomposite is for Cu^{2+} ions in the presence of other competing species in solution.

The relative selective coefficient K' , which represents the enhanced effect of imprinting on selectivity and adsorption affinity for the template onto the ion imprinted polymer/montmorillonite nanocomposite. The K' of the IIP/Mt nanocomposite against the NIP/Mt nanocomposite as determined using equation

$$K' = \frac{K_{\text{IIP/Mt}}}{K_{\text{NIP/Mt}}} \quad (4)$$

where $K_{\text{IIP/Mt}}$ and $K_{\text{NIP/Mt}}$ are the selectivity coefficients of the IIP/Mt and NIP/Mt, respectively.

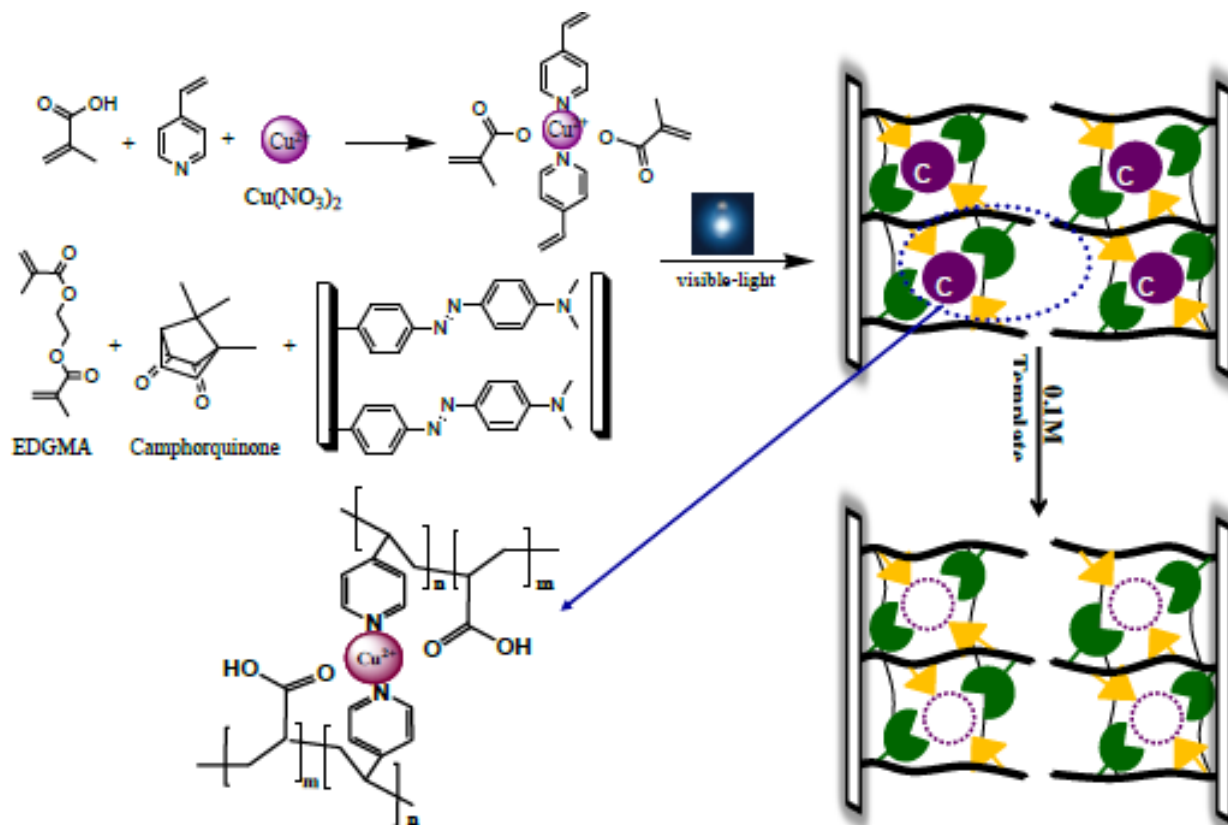
2.8. Desorption and regeneration

To estimate the reuse ability of IIP/Mt nanocomposite, synthesized adsorbant were contacted with Cu^{2+} solution for adsorption process. After adsorption, the IIP/Mt were placed in the desorption medium (1M, HNO_3 solution) and stirred for 120 minutes at room temperature. This procedure was repeated for many times until Cu^{2+} could not be detected in aqueous phase. Then, the adsorbent was washed thoroughly with double distilled water to a neutral pH to determine reusability of IIP/Mt nanocomposite, the desorption-adsorption procedure was repeated eight times using the same sorbent.

3. Results and discussion

3.1. Synthesis strategy and mechanistic aspects

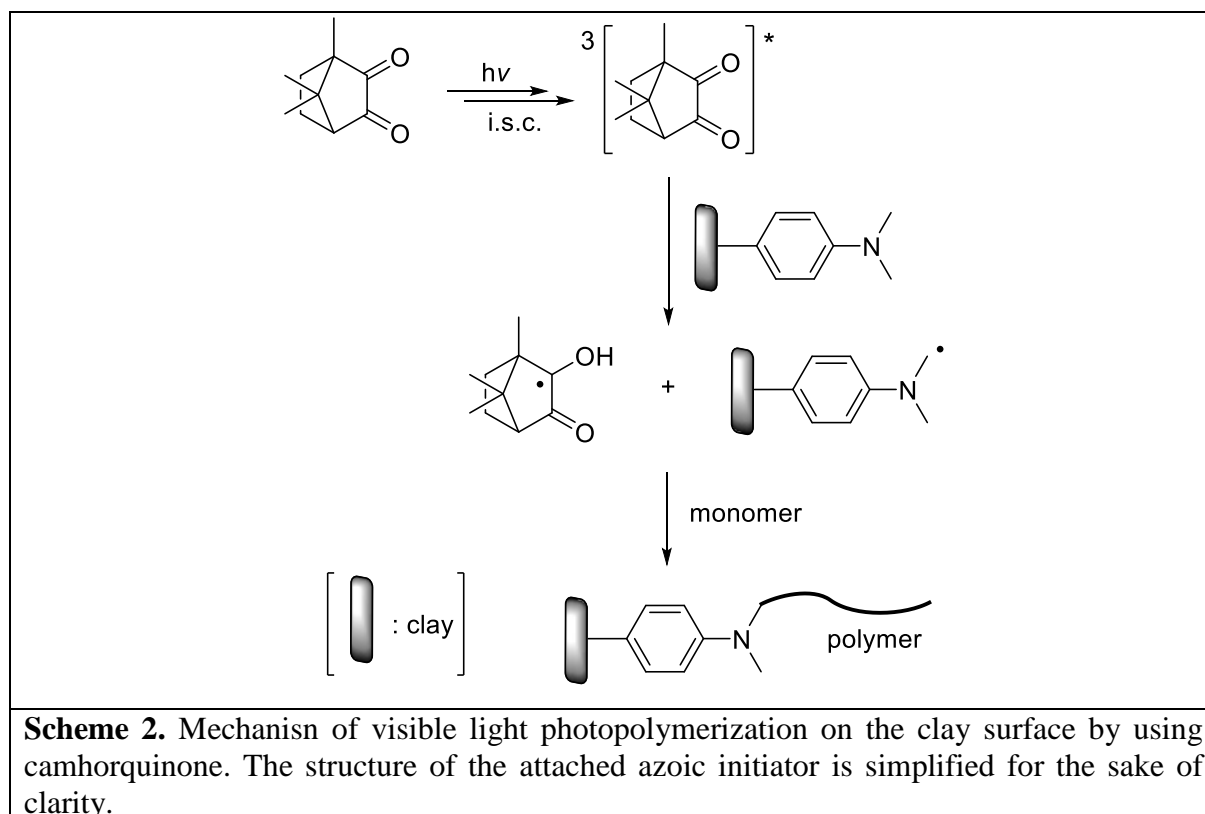
The synthesis strategy of IIP/Mt nanocomposites was carried out in two main steps starting by a simple diazonium cation exchange reaction with Na^+ (Scheme 1).



Scheme 1. Schematic representation of the synthesis procedure of Cu²⁺-IIP/ clay nanocomposite. NB: Under irradiation conditions the azo compound undergoes cis-trans isomerization. In fact, this behavior would be more beneficial since it would lead to a better intercalation.

The cation exchange reaction led to the intercalation of the diazonium cations into the clay. Heating at 60 °C was achieved in order to obtain stable aluminosilicate-aryl bond by dediazonation of the interfacial diazoether [32]. For the photopolymerization step, we have deliberately selected CQ as the photosensitizer for two reasons. First, it absorbs the light in the visible region of the electromagnetic radiation. Although there are many visible light acting photoinitiating systems [34,35,36], CQ is the safest photoinitiator and therefore, widely used in

dental applications. Secondly, upon photolysis, the triplet CQ abstracts hydrogen from hydrogen donors, i.e., amines. While the amine derived radicals initiate the polymerization CQ-H[•] radicals are not reactive towards monomers, but readily form various coupling products. This issue is particularly important for our case as chain growth occurs only on the clay surface. The overall, mechanism is presented in Scheme 2.



Separately, to form the pre-polymerization complex, $\text{Cu}(\text{NO}_3)_2$ (1equivalent) as mixed with 4-vinylpyridine (1 equiv), acrylic acid (2equiv) in DMF/ H_2O (4ml/4ml) and the mixture was shaken for 1h. This solution was then mixed with EGDMA (1equiv), diazonium-modified clay Mt_DZ (100mg) and camphorquinone (26.6mg). The suspension was purged with nitrogen for 15 min in order to prevent any unwanted reactions that inhibit the photopolymerization process. The mixture was irradiated using a Ker-Vis blue photoreactor equipped with six lamps (Philips TL-D 18 W) emitting light nominally at 400-500 nm at room temperature for 4h.

3.2. Characterization

3.2.1. XRD

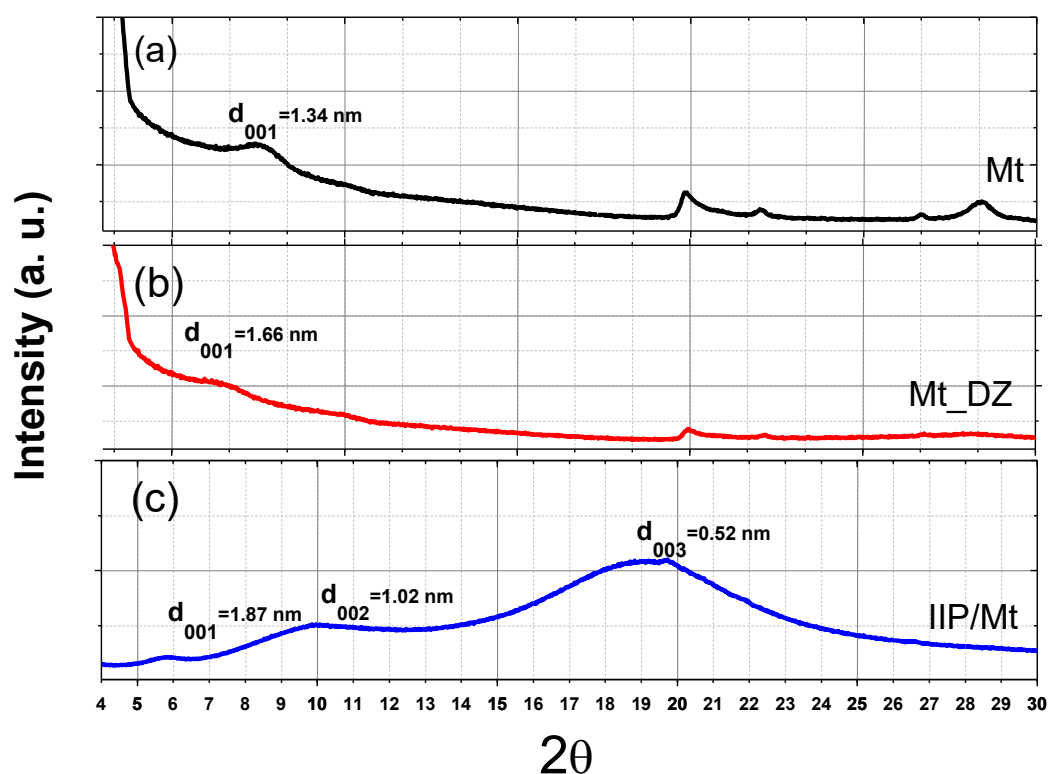


Figure 1. XRD patterns of montmorillonite Mt (g), Mt_DZ(h) and IIP/Mt(c) nanocomposite.

X-ray powder diffraction diagrams (DRX) for sodium montmorillonite clay (Mt), montmorillonite interposed with diazonium salt (Mt_DZ) and montmorillonite after photopolymerization (IIP/Mt) are shown in Figure 1.

For (Mt_DZ), the d_{001} peak position is shifted to lower values (Figure 1b) compared to the untreated clay (Figure 1a). The inter-lamellar distance of soda montmorillonite (Mt), modified montmorillonite (Mt_DZ) and montmorillonite/ionic imprinted polymer nanocomposite (IIP/Mt) were estimated from the peak (001) using the Bragg equation $n\lambda = 2d \sin\theta$. After the cation exchange reaction between the Na^+ cations and the diazonium salt, the interlayer distance was increased from 1.34 nm to 1.66 nm, which proves the intercalation of diazonium salt between the montmorillonite layers. After photopolymerization the distance d_{001} moves to the lower value of 2θ ($d_{001}=1.8$ nm), which means that after the in-situ radical photopolymerization the polymer chain is intercalated between the clay layers [37]. It is to note that Figure 1(c) showing the X-ray diffraction of the IIP/Mt nanocomposite, suggests that this adsorbent is

characterized by (001) ($1 < \ell < 4$) reflection which testifies for regular distribution of the polymer within the clay nanosheets. The positions (001), (002) and (003) peaks at $d=1.87$, 1.02 and 0.52 nm, respectively, indicate an intercalated crystalline structure of the IIP in the interlayers.

3.2.2. FTIR analysis

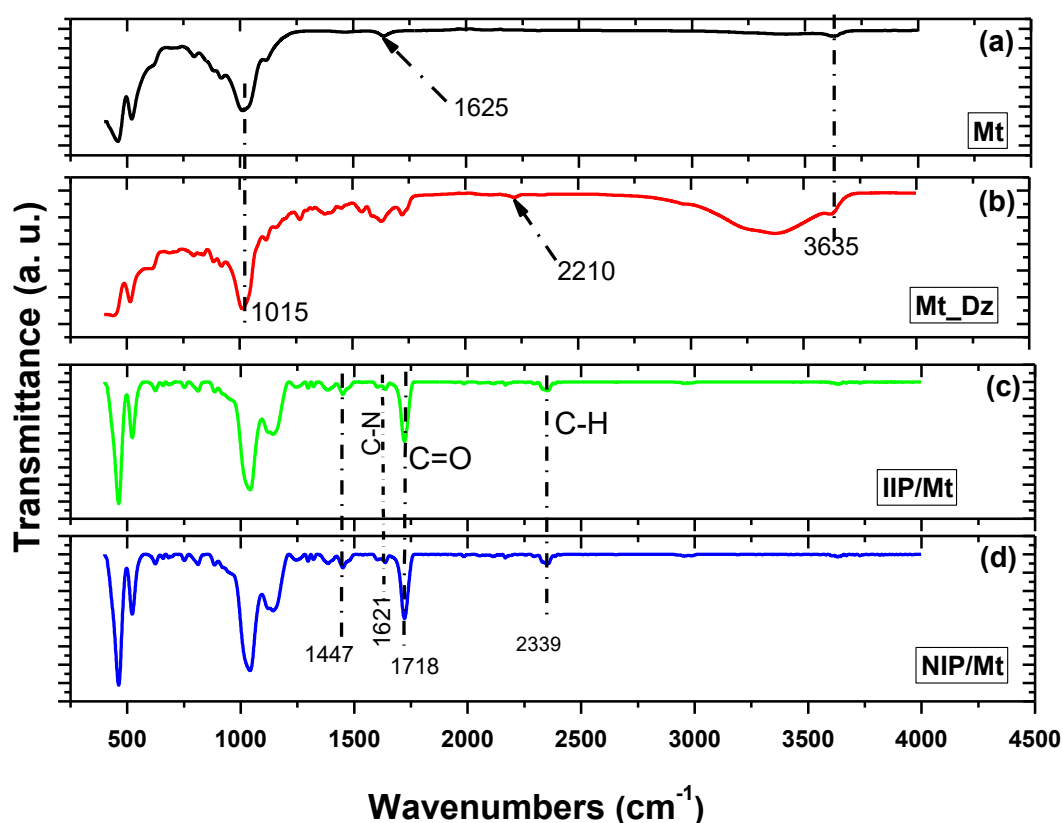


Figure 2. FTIR spectra of Mt (a), diazonium-modified montmorillonite, Mt_DZ (b), IIP/Mt (c), and NIP/Mt (d).

Figure 2 shows the FTIR spectra of Mt, Mt_DZ, IIP/Mt and NIP/Mt. The structure of the purified montmorillonite is characterized by the bands located in the $1000\text{--}1200\text{cm}^{-1}$ range assigned to Si-O-Si. The peaks at 3635 and 918cm^{-1} are in line with the dominant presence of dioctahedral smectite with (Al, Al-OH) [38]. The absorption band at 1625cm^{-1} corresponds to OH from the water molecules absorbed by the clay. After clay modification the FTIR analysis confirmed the presence of the diazonium in the clay inter spacings. FTIR data of modified clay with diazonium prove N_2^+ band at 2210cm^{-1} . Moreover, after clay modification we observe the appearance of a

band at 1621cm^{-1} assigned to the pyridine ring, and an intense band at 1447cm^{-1} which ascribed to the stretching vibration of C-N of 4-vinylpyridine. One can also note the presence of a new signal near 1718cm^{-1} corresponding to the carbonyl of the methacrylic acid. These FTIR observations are in line with the coexistence of an organic polymer fraction in the final composite material.

3.2.3. XPS analysis

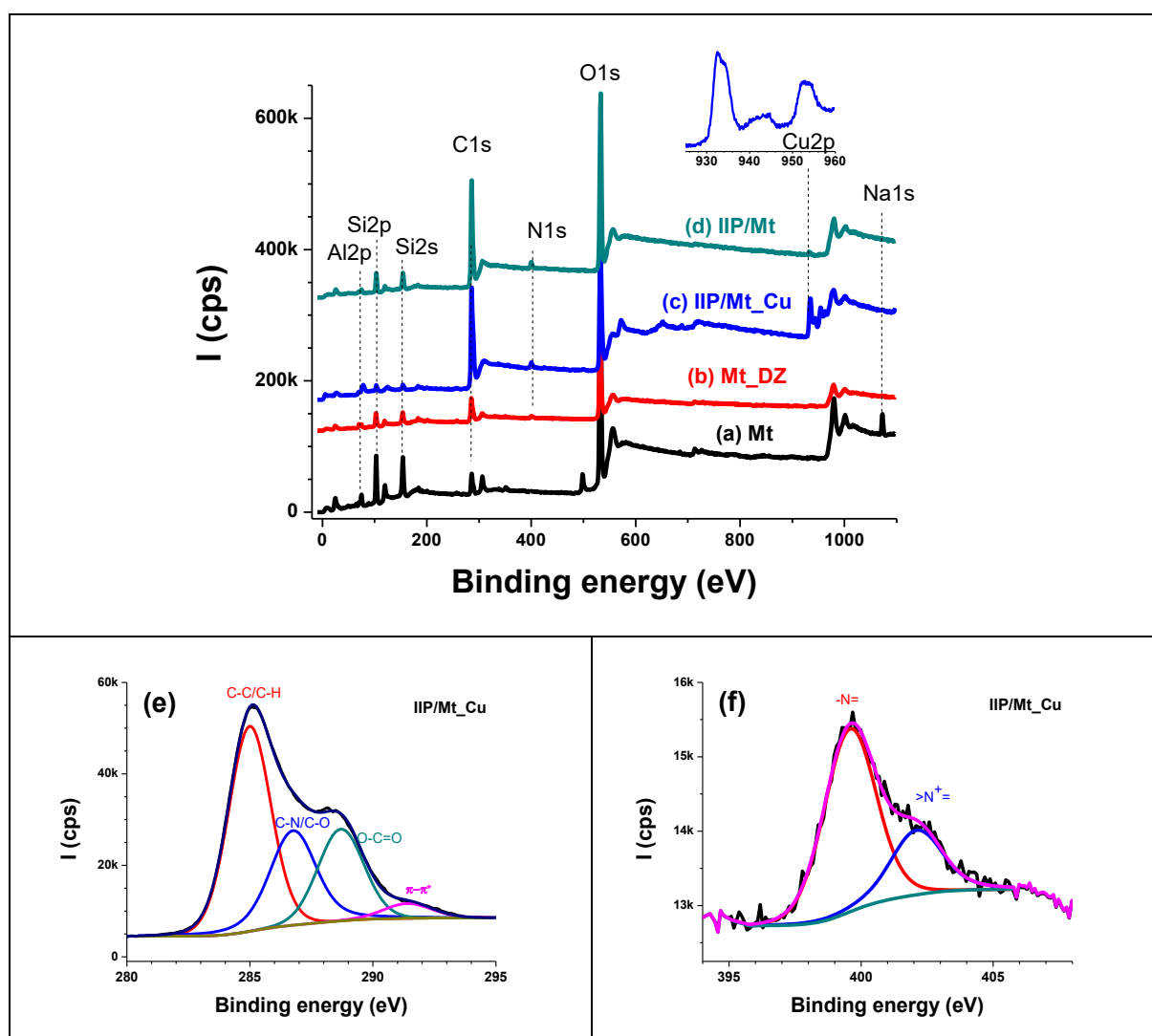


Figure 3. XPS analysis of Mt, Mt_DZ and IIP/Mt_Cu (before extraction of copper) and IIP/Mt (after extraction of copper). Survey regions: (a-d), peak-fitted C1s and N1s narrow regions of IIP/Mt_Cu: (e) and (f), respectively.

Figure 3 displays XP spectra of Mt, Mt_DZ and the nanocomposites before and after extraction of copper. The survey regions are displayed in figures 3a-d; and the main peaks are Al2p (~74

eV), Si2p (~102 eV), Si2s (152 eV), C1s (285 eV), N1s (400 eV), O1s (532 eV), Cu2p (930-960 eV) and Na1s (1072 eV). It is demonstrated here that the diazonium salt intercalates montmorillonite by cation exchange mechanism since one can see in Figure 3b the disappearance of the Na1s peak compared to the pristine clay (Figure 3a). The intercalation leads also to an increase in the C1s/Si2p intensity ratio and appearance of a tiny N1s peak (~400 eV) from the intercalated diazonium. The synthesis of the IIP/Mt_Cu results in a significant change in the survey region (Figure 3c) which exhibits sharp C1s and O1s peaks from the polymer and the existence of a Cu2p doublet. The high resolution Cu2p from IIP/Mt_Cu is shown in insert. Nitrogen is also slightly more visible as vinylpyridine was used here as a comonomer. After extraction, the Cu2p vanishes (Figure 3d).

Figures 3e and 3f display the high resolution C1s and N1s peaks of the IIP. Interestingly, the C1s shows features due to C-N (~286 eV) and the functional group COOH (~peak component at 289 eV). As far as the peak component at 292 eV is concerned, it is ascribed to aromatic species from the vinylpyridine repeat units and the diazonium-derived aryl groups attached to the clay sheets. The N1s feature from the IIP (Figure 3f) shows free and quaternized nitrogen species. The latter could be due to protonation by the COOH group of the methacrylic acid or by the OH groups from clay.

3.3. Adsorption of Cu²⁺

3.3.1. Effect of pH

The pH of the solution has a significant influence on the adsorption process as it is well-known to affect the protonation of surface functional groups. Figure 4 displays the adsorption capacity of Cu²⁺ by the IIP/Mt support; the maximum is noted at pH 5. Above this value, adsorption starts to decrease due to precipitation of copper [39]. For low pH values the adsorption of copper ions is also low this could be due to the protonation of functional sites and consequently a competition between protons from the acidic medium and Cu²⁺ ions towards the artificial receptor sites of copper. In acidic medium, adsorption increases with pH as reported for clays [40].

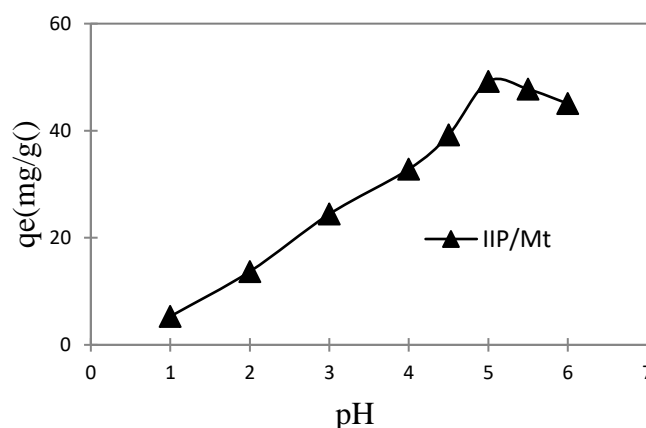


Figure 4. Effect of pH on adsorption capacity of IIP/Mt. Cu^{2+} initial concentration: 20 mg/l; adsorption time: 2h; IIP/Mt: 4 mg; room temperature.

3.3.2. Effect of contact time and a kinetic study

The effect of contact time on the adsorption of Cu^{2+} , Zn^{2+} , Pb^{2+} and Fe^{3+} on IIP/Mt and NIP/Mt nanocomposites is displayed in Figure 5. The adsorption of Cu^{2+} ions is rapid; the adsorption capacity increases with time and reaches a maximum during the first 15 minutes, then increases to saturation. The extent of adsorption of Cu^{2+} is much higher than that of Zn^{2+} , Pb^{2+} and Fe^{3+} ions (Figure 5a). This rapid equilibrium could be explained by the high affinity of complexation and geometry between Cu^{2+} ions and the cavities of the nanocomposite structure. It is known that the removal of the template from the polymer network creates smart cavities that allow us to know the shape and chemical functionality of the Template Cu^{2+} [41]. In contrast, for the NIP/Mt adsorbent, there is no significantly distinct adsorption is noted for copper. As a matter of fact, one can note in Figure 5b that the maximum adsorption is noted for zinc and not copper. From Figures 5a-b, clearly it is essential to fabricate a copper ion imprinted polymer in order to achieve selective removal of this template ion.

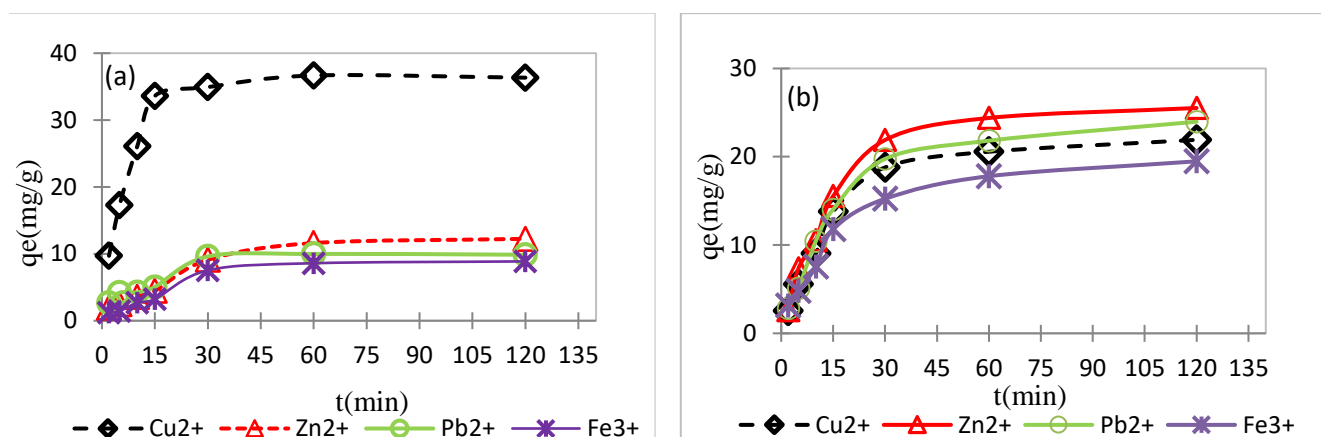


Figure 5. Effect of contact time on the removal Cu^{2+} , Zn^{2+} , Pb^{2+} and Fe^{3+} by IIP/Mt(a), and NIP/Mt(b). Conditions: initial Cu^{2+} concentration = 20mg/L, and pH=5.

To study the adsorption process, pseudo-first order and pseudo-second order models were used to control the check adsorption kinetics of IIP/Mt and NIP/Mt.

The pseudo-first-order and pseudo-second-order models are described as equations (5) [42] and (6) [43], respectively.

$$\log(q_e - q_t) = \log q_e - \frac{k_1}{2.303} t \quad (5)$$

$$\frac{t}{q} = \frac{1}{k_2 q_e^2} + \frac{t}{q_e} \quad (6)$$

Where q_t (mg/g) and q_e (mg/g) are the adsorption capacities of metal ions on IIP/Mt and NIP/Mt at time t and equilibrium, respectively; k_1 (L/min) and k_2 (g/mg min) are the first order and second order adsorption constants, respectively.

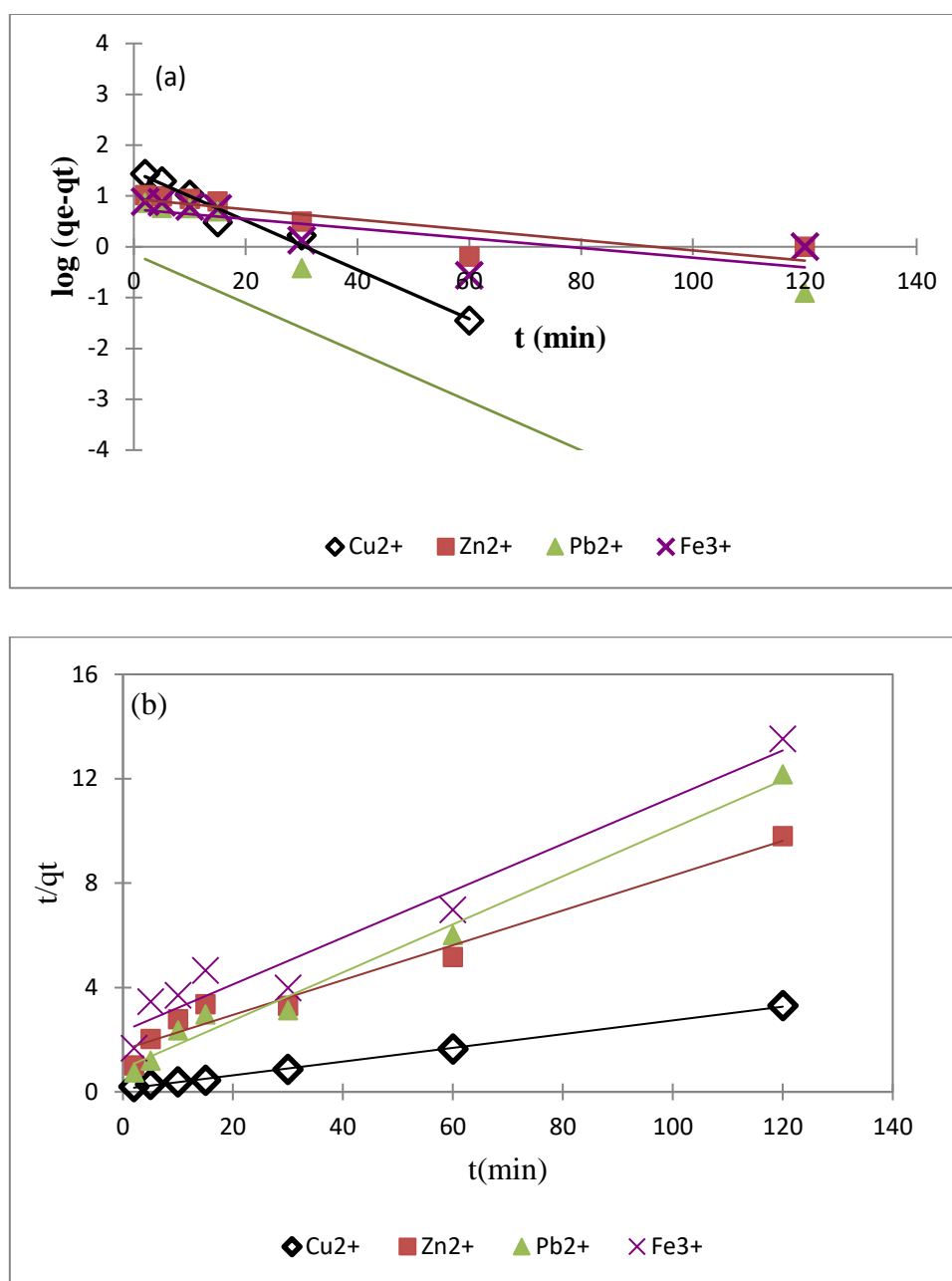


Figure 6. Pseudo-first-order (a), and pseudo-second-order (b) kinetic model applied to the adsorption of Cu²⁺, Zn²⁺, Pb²⁺ and Fe³⁺ onto IIP/Mt nanocomposites.

The kinetic modeling for the adsorption of metal ions on IIP/Mt nanocomposites is shown in Figure 6 and the adsorption kinetics constants and the correlation coefficient values R^2 are summarized in Table 1. The values of the correlation coefficient R^2 of the pseudo-second-order model are significantly higher than those of the other models and closer to unity which accounts

for pseudo-second order mechanism of the adsorption process on the IIP/Mt nanocomposite. It follows that chemisorption is the driving force for the adsorption process on the actual IIP/Mt nanocomposite [44].

Table1. Kinetic parameters of the pseudo-first-order and the pseudo-second –order rate equations for ions metals adsorption on IIP/Mt nanocomposites.

Ions	Pseudo-first- order			Pseudo-second –order		
	$q_e(\text{mg/g})$	$K_1(\text{L/min})$	R^2	$q_e(\text{mg/g})$	$K_2 \cdot 10^{-2}(\text{g/mg min})$	R^2
Cu^{2+}	30.130	0.110	0.978	38.461	0.625	0.998
Zn^{2+}	8.689	0.023	0.728	15.151	0.269	0.966
Pb^{2+}	9.856	0.110	0.134	10.869	0.945	0.984
Fe^{3+}	5.457	0.0207	0.519	11.236	0.340	0.954

3.3.3. Adsorption isotherms

Figure 7 shows the effects of aqueous phase Cu^{2+} concentrations on equilibrium adsorption capacity on IIP/Mt. The adsorption capacity increases with increasing concentration in the aqueous phase. Adsorption of the metal ion saturates at 23.562 mg/g (q_{max}). In this study the adsorption isotherm is applied to study the interactions between metal ions and the active sites of our adsorbent (IIP/Mt). The adsorption isotherm is expressed for an adsorbent-adsorbate pair as a function of concentration. The adsorption isotherm of Cu^{2+} ions was checked whether it fits the Langmuir [45] or Freundlich [46] isotherm models (see Figure 8) as described by equations (7) and (8), respectively. The Langmuir isotherm theory assumes that adsorption is single-layer and takes place at homogeneous sites specific to the adsorbent and the Freundlich isotherm assumes that adsorption is multi-layer and that the surface of the adsorbent is heterogeneous.

$$\frac{C_e}{q_e} = \frac{1}{Q_m K_L} + \frac{C_e}{Q_m} \quad (7)$$

$$\log q_e = \log K_F + \frac{1}{n} \log C_e \quad (8)$$

Where q_e (mg/g) is the adsorbed amount at equilibrium, C_e is the equilibrium concentration of the metal ions (mg/L), K_L (L/mg), $K_F(\text{mg}^{1-1/n}/\text{gL}^{1/n})$ are the Langmuir equilibrium and the

Freundlich constants, respectively; qm the maximum adsorption capacity (mg/g), n is the heterogeneity factor, and $1/n$ value is related to the sorption intensity.

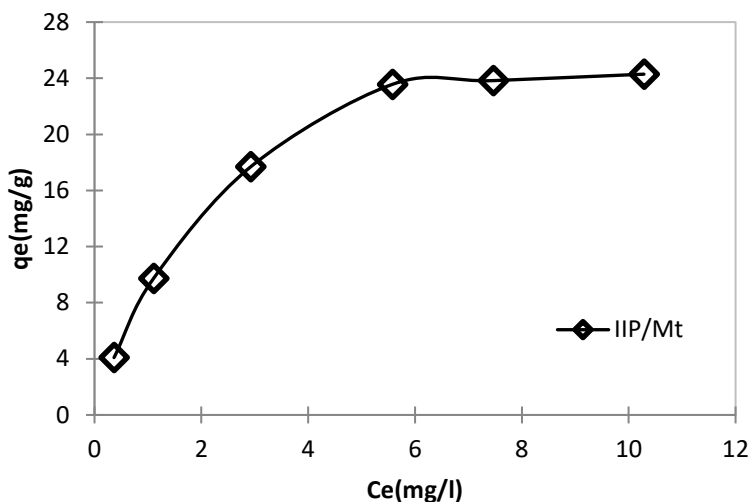


Figure 7. Adsorption isotherms of Cu^{2+} on IIP/Mt nanocomposite at pH 5.

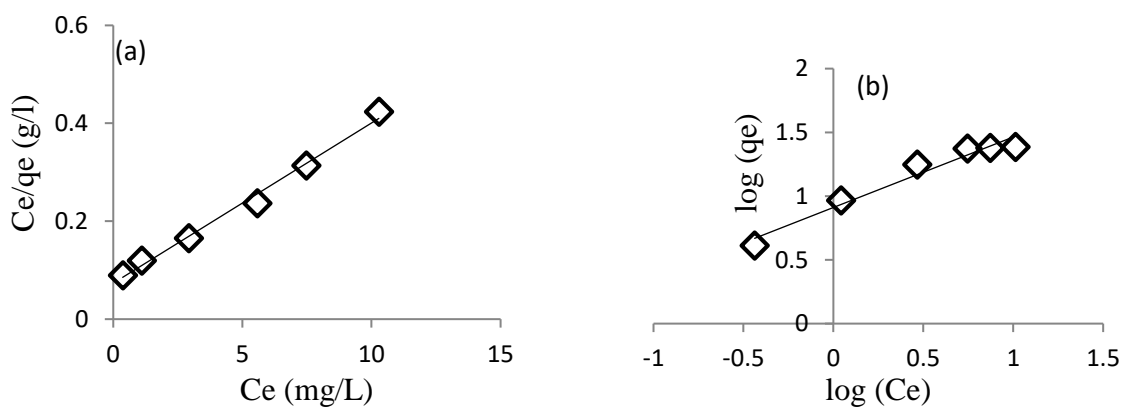


Figure 8. Isotherms models for adsorption of Cu^{2+} on IIP/Mt at room temperature: Langmuir (a), and Freundlich (b).

Table 2 lists all isotherm parameters. The data show that Langmuir model (Figure 8a) is more suitable to describe the adsorption reaction of Cu^{2+} on the IIP/Mt with the experimental data with higher R^2 values. Therefore, these results imply that the adsorption process of IIP/Mt is surface monolayer adsorption and the adsorption sites are homogeneous [47,48].

Table2. Adsorption equilibrium constants for Langmuir and Freundlich isotherms.

Adsorbents	Metal ion	Langmuir isotherm			Freundlich isotherm		
		qm(mg/g)	K _L (L/mg),	R ²	K _F (mg ^{1-1/n} /gL ^{1/n})	n	R ²
IIP/Mt	Cu ²⁺	31.25	3.555	0.991	8.128	1.811	0.958

3.3.4. Adsorption selectivity

To evaluate the selective properties of the IIP/Mt and NIP/Mt nanocomposites, adsorption of Cu²⁺ was conducted in the presence of competitive ions in binary systems. In our work, the binary solute solutions, including Cu²⁺/Zn²⁺, Cu²⁺/Pb²⁺ and Cu²⁺/Fe³⁺ were studied to explore the selectivity to template Cu²⁺ at room temperature. The distribution coefficients (K_d), the selectivity coefficients (K) and the relative selectivity coefficients (K') were calculated (see Table 3). It is noted that the distribution coefficient value of Cu²⁺ is greater than that of the other metal ions. Therefore, high selectivity coefficients were determined for IIP/Mt and NIP/Mt nanocomposites: 10.308, 6.515 and 8.524 for Cu²⁺/Zn²⁺, Cu²⁺/Pb²⁺ and Cu²⁺/Fe³⁺, respectively. The selectivity for Cu²⁺ is due to the ion imprints shaped in the polymer network of the nanocomposite. The geometry, charge and size of the prints account for the selective recognition of Cu²⁺ ions over the other cationic competitors.

Table3. Selectivity adsorption parameters for IIP/Mt and NIP/Mt nanocomposites.

Metals	IIP/Mt		NIP/Mt		K'
	k _d	k	k _d	k	
Cu²⁺	29.904		2.073		
Zn²⁺	3.657	10.308	21.029	0.0985	104.568
Pb²⁺	3.555	6.515	28.808	0.0719	90.538
Fe³⁺	8.152	8.524	7.269	0.285	29.891

3.3.5. Regeneration of IIP/Mt

In order to evaluate the reusability and the renewability of the synthesized sorbent, several adsorption-desorption cycles were carried out on the same sample of IIP/Mt nanocomposite d at the same Cu^{2+} concentration of 20 mg/l. The desorption of the Cu^{2+} ions adsorbed from the IIP/Mt nanocomposites was carried out using a 2M HNO_3 solution. Several cycles of adsorption-desorption were applied to the IIP/Mt adsorbent. The results displayed in Figure 9 permit to claim stability of the IIP/Mt nanocomposite adsorbent which could be regenerated without significant loss of performance. Indeed, up to 8 adsorption/desorption cycles were applied to the robust adsorbent designed so far which did not show any sign of decrease in performances.

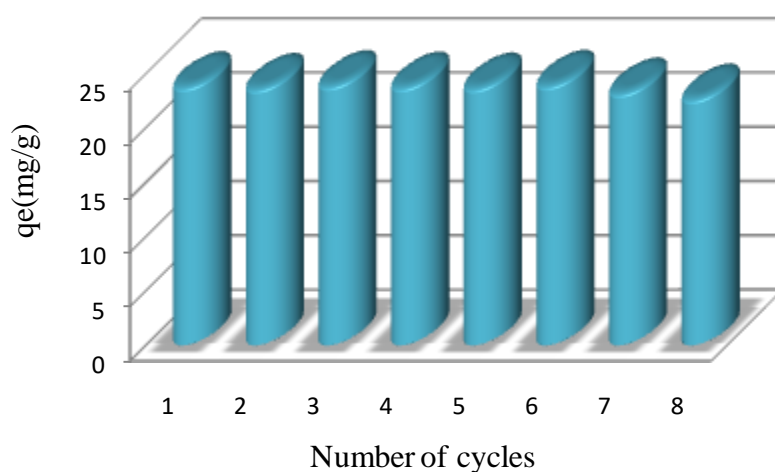


Figure 9. Recycling of the IIP/Mt in the removal of Cu^{2+} from aqueous relations ($C_0= 20$ mg/l, pH=5, RT).

4-Conclusion

Montmorillonite-based ion imprinted polymer nanocomposite was prepared by radical photopolymerization under visible light exposure. The pre-polymerization complex was prepared by mixing $\text{Cu}(\text{NO}_3)_2$ and functional monomers of 4-VP and MAA mixed in DMF/ H_2O . Then, this solution was mixed with the cross-linker (EDGMA), photoinitiator (camphorquinone, CQ) and modified montmorillonite by diazonium (Mt_DZ). We show that

diazonium salt is a good intercalant for clay and for triggering in situ radical photopolymerization. In this study, Cu²⁺-imprinted polymer/ montmorillonite nanocomposite was successfully prepared and applied for the pre-concentration and determination of Cu²⁺ ions in aqueous solutions. The experimental data followed the Langmuir isothermal model and pseudo-second order kinetics. In addition, these artificial sites shaped to accommodate Cu²⁺ could uptake copper at high extent compared to the competing metal ions Zn²⁺, Pb²⁺ and Fe³⁺, but also much more than non-imprinted polymer/montmorillonite nanocomposite. The selectivity with other ions confined that IIP/Mt showed high specific Cu²⁺ ions.

This work demonstrates for the very first time the efficiency of diazonium salt to initiate visible light radical photopolymerization within the interlayer spacings of layered aluminosilicates. The method could be applied to other nanomaterials which could serve as nanoscale platforms to be coated by ion or molecularly imprinted polymers.

Author Contributions: Conceptualization of the research work by RM, SA, MMC and YY; Methodology by RM, GY, AA, YY, MMC; Validation by RM, SH, AA, YY, MMC; Formal Analysis by RM, AA, GY, SH, MMC; Writing of Original Draft was done by RM and MMC; Writing-Review & Editing, RM, MMC, YY; Supervision, SA, MMC and YY.

Conflicts of Interest: “The authors declare no conflict of interest.”

References

- [1] Tóth, G.; Hermann, T.; Silva, M.R.Da.; Montanarella, L. Heavy metals in agricultural soils of the European Union with implications for food safety. *Environ. Int.* **2016**, *88*, 299-309
- [2] Duruibe, J. O.; Ogwuegbu, M. O. C.; Egwurugwu, J. N. Heavy metal pollution and human biotoxic effects. *Int. J. Phys. Sci.* **2007**, *2*, 112-118.
- [3] Khan, A., Khan, S., Khan, M.A.; Qamar, Z.; Waqas, M. The uptake and bioaccumulation of heavy metals by food plants, their effects on plants nutrients, and associated health risk: a review. *Environ. Sci. Pollution Res.* **2015**, *22*, 13772–13799.
- [4] http://www.who.int/ipcs/assessment/public_health/lead/en/ Last accessed 20 November 2018.
- [5] Kamaruddin, N.H.; Bakar, A.A.A.; Mobarak, N.N.; Zan, M. S. D.; Arsad, N. Binding affinity of a highly sensitive Au/Ag/Au/Chitosan-Graphene oxide sensor based on direct detection of Pb²⁺ and Hg²⁺ ions. *Sensors*. 2017, *17*, 2277; doi:10.3390/s17102277.
- [6] Lo, M.; Pires, R.; Diaw, K.; Gningue-Sall, D.; Oturan, M. A.; Aaron, J.-J.; Chehimi, M. M. Diazonium salts: versatile molecular glues for sticking conductive polymers to flexible electrodes, *Surfaces* **2018**, *1*, 43-58; <https://doi.org/10.3390/surfaces1010005>
- [7] Bailey, S. E.; Olin, T.J.; Bricka, R.M.; Adrian, D.D. A review of potentially low-cost sorbents for heavy metals. *Wat. Res.* 1999, *33*, 2469-2479.
- [8] Abollino, O.; Aceto, M.; Malandrino, M.; Sarzanini, C.; Mentasti, E. Adsorption of heavy metals on Na-montmorillonite. Effect of pH and organic substances. *Water Res.* 2003, *37*, 1619–1627.
- [9] (a) de Paiva, L.B.; Morales, A. R.; Díaz, F. R.V. Organoclays: Properties, preparation and applications, *Appl. Clay Sci.* **2008**, *42*, 8-24 / (b) Yao, H.; Zhu, J.; Morgan, A.B.; Wilkie, C.A. Crown ether-modified clays and their polystyrene nanocomposites. *Polym. Eng. Sci.* **2002**, *42*, 1808–1814.
- [10] Tchinda, A. J.; Ngameni, E.; Kenfack, I. T.; Walcarius, A. One-Step Preparation of Thiol-Functionalized Porous Clay Heterostructures: Application to Hg(II) Binding and Characterization of Mass Transport Issues. *Chem. Mater.* **2009**, *21*, 4111–4121
- [11] Salmi, Z.; Benzarti, K.; Chehimi, M. M. Diazonium cation-exchanged clay: an efficient, unfrequented route for making clay/polymer nanocomposites. *Langmuir*, **2013**, *29*, 13323–13328.
- [12] Jlassi, K.; Chandran, S.; Mičušik, M.; Benna-Zayani, M.; Yagci, Y.; Thomas, S.; Chehimi, M. M. Poly(glycidyl methacrylate)-grafted clay nanofiller for highly transparent and mechanically robust epoxy composites. *Eur. Polym. J.* **2015**, *72*, 89–101.
- [13] Msaadi, R.; Gharsalli, A.; Mahouche-Chergui, S.; Nowak, S.; Salmi, H.; Carbonnier, B.; Ammar, S.; Chehimi, M.M. Reactive and functional clay through UV-triggered thiol-ene interfacial click reaction. *Surf. Interface Anal.* **2016**, *48*, 385-693.
- [14] Fei, Y.; Liu, C.; Li, F.; Chen, M.; Tong, H.; Liu, C.; Liao, C.; Combined modification of clay with sulfhydryl and iron: Toxicity alleviation in Cr-contaminated soils for mustard (*Brassica juncea*) growth. *J Geochem Explor.* **2017**, *176*, 2–8.
- [15] Monzavi, A.; Montazer, M.; Malek, R.M.A. A Novel Polyester Fabric Treated with Nanoclay/Nano TiO₂/PAMAM for Discoloration of Reactive Red 4 from Aqueous Solution Under UVA Irradiation, *J. Polym. Environ.* **2017**, *25*, 1321-1334.

- [16] Jlassi, K.; Abidi, R.; Benna, M.; Chehimi, M.M.; Kasak, P.; Krupa, I. Bentonite-decorated calix [4] arene: A new, promising hybrid material for heavy-metal removal; *Appl Clay Sci.* **2018**, *161*, 15-22
- [17] Kamboh, M. A.; Memon, S.; Zardari, L.A.; Nodeh, H.R.; Sherazi, S.T.H.; Yilmaz, M.; Removal of toxic metals from canola oil by newly synthesized calixarene-based resin; *Turk J Chem.* **2018**, *42*, 918 – 928.
- [18] Unuabonah, E. I.; Taubert, A. Clay–polymer nanocomposites (CPNs): Adsorbents of the future for water treatment, *Appl. Clay Sci.* **2004**, *99*, 83–92.
- [19] Nese, A.; Sen, S.; Tasdelen, M. A.; Nugay, N.; Yagci, Y. Clay-PMMA nanocomposites by photoinitiated radical polymerization using intercalated phenacyl pyridinium salt initiators. *Macromol. Chem. Phys.* **2006**, *207*, 820–826.
- [20] (a) Tasdelen, M. A. ; Van Camp, W.; Goethals, E.; Dubois, P.; Du Prez, F.; Yagci, Y. Polytetrahydrofuran/clay nanocomposites by in situ polymerization and “click” chemistry processes. *Macromolecules* **2008**, *41*, 6035–6040 / (b) Akat, H.; Tasdelen, M. A.; Du Prez, F.; Yagci, Y. Synthesis and characterization of polymer/clay nanocomposites by intercalated chain transfer agent. *Eur. Polym. J.* **2008**, *44*, 1949–1954.
- [21] (a) Oral, A. Tasdelen, M. A.; Demirel, A. L.; Yagci, Y. Poly (cyclohexene oxide)/clay nanocomposites by photoinitiated cationic polymerization via activated monomer mechanism. *J. Polym. Sci. Part A: Polym. Chem.* **2009**, *47*, 5328–5335. / (b) Yenice, Z.; Tasdelen, M. A.; Oral, A.; Guler, C.; Yagci, Y. Poly(styrene-*b*-tetrahydrofuran)/clay nanocomposites by mechanistic transformation. *J. Polym. Sci. Part A: Polym. Chem.* **2009**, *47*, 2190–2197 / (c) Oral, A.; Tasdelen, M. A.; Demirel, A. L.; Yagci, Y. *Polymer* **2009**, *50*, 3905–3910.
- [22] Tasdelen, M. A.; Kreutzer, J. ; Yagci, Y. In situ synthesis of polymer/clay nanocomposites by living and controlled/living polymerization. *Macromol. Chem. Phys.* **2010**, *211*, 279–285.
- [23] Demir, K. D.; Tasdelen, M. A.; Uyar, T.; Kawaguchi, A. W.; Sudo, A.; Endo, T.; Yagci, Y. Synthesis of polybenzoxazine/clay nanocomposites by in situ thermal ring-opening polymerization using intercalated monomer. *J. Polym. Sci. Part A: Polym. Chem.* **2011**, *49*, 4213–4220 / (b) Altinkok, C.; Uyar, T.; Tasdelen, M. A.; Yagci, Y. In situ synthesis of polymer/clay nanocomposites by type II photoinitiated free radical polymerization. *J. Polym. Sci. Part A: Polym. Chem.* **2011**, *49*, 3658–3663.
- [24] Pan, J.; Zou, X.; Yan, Y.; Wang, X.; Guan, W.; Han, J.; Wu, X. An ion-imprinted polymer based on palygorskite as a sacrificial support for selective removal of strontium (II). *Appl. Clay Sci.* **2010**, *50*, 260-265.
- [25] Branger, C.; Meouche, W.; Margailan, A. Recent advances on ion-imprinted polymers. *React. Func. Polym.* **2013**, *73*, 859–875.
- [26] Uddin, M.K. A review on the adsorption of heavy metals by clay minerals, with special focus on the past decade. *Chem. Eng. J.* **2017**, *308*, 438–462.
- [27] Hande, P. E.; Samui, A. B.; Kulkarni, P. S. Highly selective monitoring of metals by using ion-imprinted polymers, *Environ. Sci. Pollut. Res.* **2015**, *22*, 7375–7404.
- [28] Xu, X.; Wang, M.; Wu, Q.; Xu, Z.; Tian, X. Synthesis and application of novel magnetic ion-imprinted polymers for selective solid phase extraction of cadmium (II). *Polymers* **2017**, *9*, 360; <https://doi.org/10.3390/polym9080360>
- [29] Nitrate ion selective electrode based on ion imprinted poly(N-methylpyrrole). Bomar, E. M.; Owens, G. S. ; Murray, G. M. *Chemosensors* **2017**, *5*, 2 <https://doi.org/10.3390/chemosensors5010002>

- [30] A new ion-imprinted chitosan-based membrane with an azo-derivative ligand for the efficient removal of Pd(II)
- Di Bello, M. P.; Lazzoi, M. R.; Mele, G.; Scorrano, S.; Mergola, L.; Del Sole, R. *Materials* **2017**, *10*, 1133; <https://doi.org/10.3390/ma10101133>
- [31] Ait-Touchente, Z.; Sakhraoui, H.E.E.Y.; Fourati, N.; Zerrouki, C.; Maouche, N.; Touzani, R.; Yaakoubi, N.; Chehimi, M. M. Zinc oxide nanorods wrapped with ion-imprinted polypyrrole polymer for picomolar selective and electrochemical detection of mercury II ions. *Proceedings* **2018**, *2*, 1004; <https://doi.org/10.3390/proceedings2131004>
- [32] Msaadi, R.; Ammar, S.; Chehimi, M.M.; Yagci, Y. Diazonium-based ion-imprinted polymer/clay nanocomposite for the selective extraction of lead (II) ions in aqueous media. *Eur. Polym. J.* **2017**, *89*, 367-38.
- [33] Bakas, I.; Yilmaz, G.; Ait-Touchente, Z.; Lamouri, A.; Lang, P.; Battaglini, N.; Carbonnier, B.; Chehimi, M. M.; Yagci, Y. Diazonium salts for surface-confined visible light radical photopolymerization. *J. Polym. Sci. A Polym. Chem.* **2016**, *54*, 3506–3515.
- [34] (a) Salmi, H.; Tar, H.; Ibrahim, A.; Ley, C.; Allonas, X. Squarylium-triazine dyad as a highly sensitive photoradical generator for red light, *Eur. Polym. J.*, **2013**, *49*, 2275-2279 / (b) Jing Zhang, Nicolas Zivic, Frédéric Dumur, Pu Xiao, Bernadette Graff, Jean-Pierre Fouassier, Didier Gignes, Jacques Lalevée. Naphthalimide-Tertiary Amine Derivatives as Blue-Light-Sensitive Photoinitiators, *ChemPhotoChem* **2018**, *2*, 481-489.
- [35] (a) Eibel, A.; Radebner, J.; Haas, M.; Fast, DE; Freissmuth, H.; Stadler, E.; Faschauner, P.; Torvisco, A.; Lamparth, I.; Moszner, N.; Stueger, H.; Gescheidt, G. From mono- to tetraacylgermanes: extending the scope of visible light photoinitiators, *Polym. Chem.*, **2018**, *9*, 38-47. / (b) Mitterbauer, M.; Knaack, P.; Naumov, S.; Markovic, M.; Ovsianikov, A.; Moszner, N.; Liska, R. Acylstannanes: cleavable and highly reactive photoinitiators for radical photopolymerization at wavelengths above 500 nm with excellent photobleaching behavior, *Angew. Chem. Int. Ed.*, **2018**, *57*, 12146-12150.
- [36] (a) Yilmaz, G.; Aydogan, B.; Temel, G.; Arsu, N.; Moszner, N.; Yagci, Y. Thioxanthone-Fluorenes as Visible Light Photoinitiators for Free Radical Polymerization. *Macromolecules*, **2010**, *43*, 4520-4526. / (b) Tunc D, Yagci Y, *Polymer Chemistry*, **2011**, *2*(11), 2557-2563 / (c) Kiskan, B.; Zhang, J.; Wang, X.; Antonietti, M.; Yagci, Y. Mesoporous graphitic carbon nitride as a heterogeneous visible light photoinitiator for radical polymerization, *ACS Macro Lett.*, **2012**, *1*, 546-549.
- [37] Salmi-Mani, H.; Ait-Touchente, Z.; Lamouri, A.; Carbonniera, B.; Caronc, J.F.; Benzarti, K.; Chehimi, M.M. Diazonium salt-based photoiniferter as a new efficient pathway to clay-polymer nanocomposites. *RSC Adv.* **2016**, *6*, 88126-88134
- [38] Caillère, S.; Henin, S.; Rautureau, M. *Minéralogie Des Argiles*. vol. I–II, Masson, Paris (France), 1982
- [39] Aziz, H. A.; Adlan, M. N.; Ariffin, K. S. Heavy metals (Cd, Pb, Zn, Ni, Cu and Cr(III)) removal from water in Malaysia: Post treatment by high quality limestone. *Bioresource Technol.* **2008**, *99*, 1578-1583.
- [40] (a) Farrah, H.; Pickering, W. F. The sorption of copper species by clays. I kaolinite. *Aust. J. Chem.* **1976**, *29*, 1167-76. / (b) Hyun, S.P.; Cho, Y. H.; Kim, S. J.; Hahn, P. S. Cu(II) sorption mechanism on montmorillonite: an electron paramagnetic resonance study. *J. Colloid Interface Sci.* **2000**, *222*, 254-261.
- [41] Karabork, M.; Ersoz, A.; Denizli, A.; Say, R. Polymer-clay nanocomposite iron traps based on intersurface ion-imprinting. *Ind. Eng. Chem. Res.* **2008**, *47*, 2258-2264.

-
- [42] Wang, Y.; Mu, Y.; Zhao, Q.B.; Yu, H.Q. Isotherms, kinetics and thermodynamics of dye biosorption by anaerobic sludge. *Sep. Purif. Technol.* **2006**, *50*, 1-7.
- [43] Ho, Y. S.; McKay, G. Pseudo-second order model for sorption processes. *Process Biochem.*, **1999**, *34*, 451–465.
- [44] Ho, Y. S.; McKay, G. A comparison of chemisorption kinetic models applied to pollutant removal on various sorbents. *Process Safety Environ. Protection*, **1998**, *76*, 332 – 340.
- [45] Langmuir, I. The adsorption of gases on plane surfaces of glass, mica and platinum. *J. Am. Chem. Soc.* **1918**, *40*, 1361-1403.
- [46] Freundlich, H.M.F. Over the adsorption in solution. *J. Phys. Chem.* **1906**, *57*, 385-470.
- [47] Sun, Y.; Yang, S.; Chen, Y.; Ding, C.; Cheng, W.; Wang, X. Adsorption and desorption of U(VI) on functionalized graphene oxides: a combined experimental and theoretical study; *Environ. Sci. Technol.* **2015**, *49*, 4255-4262.
- [48] Zhao, H.; Ye, Y.; Cao, S.; Dai, J.; Li, L. Synthesis and properties of cadmium(ii)-imprinted polymer supported by magnetic multi-walled carbon nanotubes. *Anal. Methods.* **2014**, *6*, 9313-9320.